An energy model of droplet impingement on an inclined wall under isothermal and non-isothermal environments

Jiachen Zhai, Seong-Young Lee, Nitisha Ahuja, Le Zhao, Xiucheng Zhu

Department of Mechanical Engineering-Engineering Mechanics, Michigan Technological University

1400 Townsend Drive, Houghton, MI 49931

Abstract

The study of spray-wall interaction is of great importance to understand the dynamics that occur during fuel impingement onto the chamber wall or piston surfaces in internal combustion engines. It is found that the maximum spreading length of an impinged droplet can provide a quantitative estimation of heat transfer and energy transformation for spray-wall interaction. Furthermore, it influences the air-fuel mixing and hydrocarbon and particle emissions at combusting conditions. In this paper, an analytical model of different droplet-wall impingement conditions is developed in terms of β_m (dimensionless maximum spreading length, the ratio of maximum spreading length to initial droplet diameter) to understand the detailed impinging dynamic process. These conditions are grouped as: a single diesel droplet impinging on the wall with different inclined angles (α); cold wall - heated droplet and heated wall - cold droplet impingement when inclined angle of the wall is 0°, respectively. The analytical model is built up based on the energy conservation that considers kinetic energy, gravitation energy, and surface energy before impingement, as well as viscous dissipation, gravitation energy, adhesion energy, deformation energy, and heat energy after impingement. The experimental work of diesel droplet impinging on an inclined wall is performed at a certain range of the Weber number (*We* of 33 to 420) with various inclined angles (α of 0° to 45°), while for inclined angle is 0°, droplet and wall temperature are varied from 25°C to 150°C to study the effects of the inclined angle and temperature on the temporal evolution of the post-impingement characteristics (i.e. droplet spreading length, dynamic contact angle). The analytical model is validated and evaluated at the aforementioned experimental operating points. The validated model can be employed to predict maximum spreading length of the droplet impinged on the wall. It is further utilized to determine the transition from capillary regime to kinetic regime, then to viscous regime at different inclined angle of the wall.

Keywords: droplet-wall impingement; inclined angle; temperature; energy conservation; spreading length

1. Introduction

The impingement of liquid fuel spray on chamber wall or piston surface in internal combustion engines is a very common phenomenon. In direct injection (DI) engines, the liquid film is formed during fuel impinging onto the chamber wall or piston surface, affecting the air-fuel mixing process significantly and subsequently the hydrocarbon and particulate matter emissions formation. For the port fuel injection (PFI) engines, the fuel film formed due to spray-wall interaction may cause time lag in the air-fuel ratio control, leading to the increase of fuel consumption [1-4]. Therefore, the study of the spray impingement on the chamber wall or piston surface is important to be fully understood. As the spray-wall impingement is known to require a detailed record of droplet size, number, and velocity near the impinged surface, of either primary or secondary droplets, the individual droplet impingement on the solid wall has been extensively used to describe the spray impact characteristics and predict the interaction outcomes [4-7].

The fluid dynamic phenomenon during droplet impingement on a solid wall depends upon many parameters, such as fuel properties (surface tension, viscosity, wettability, and density) and operating conditions (wall temperature, ambient temperature, and ambient pressure) [6, 8]. The impingement process is found to be the function of droplet impact energy that is usually represented by non-dimensional parameters of Weber number (*We*) or Reynolds number (*Re*), characterizing the relative magnitude of the forces acting on the droplet [9, 10]. The Ohnesorge number *Oh* defined by Wolfgang won Ohnesorge [11] is another non-dimensional number that relates the viscous force to the inertial and surface tension forces. Larger *Oh* indicates a greater influence of the viscosity with respect to the inertial and surface tension forces. In addition, the

maximum spreading diameter after droplet impingement on the solid wall provides a quantitative estimation of heat transfer from the solid to the liquid droplet and energy transformation [4].

Regarding droplet-wall impingement, Stow et al. [12] carried out an experimental investigation by studying water droplets impinging on a roughened aluminum surface, to understand the droplet-wall interaction phenomenon and its dependence on the *We* and *Re* of liquid fuel and surface roughness. They found a correlation between *We* and *Re* to indicate the interaction outcome of non-splashing and splashing. Zhao et al. [4] experimentally studied the dynamic process of the single droplet impinging on a flat plate at various operating conditions, including different wall temperature and four different test fuels, as well as various *We*. The new correlation of deposition-splash criteria during droplet impingement was developed. Zhu et al. [13] investigated the effect of heat transfer and thermophysical properties on dynamics of single diesel droplet impinging on a flat plate at the isothermal and non-isothermal conditions. The results showed that the heat transfer and thermophysical properties have an essential effect on the post impingement droplet dynamics and the significant differences in the spatial-temporal evolution of impinged droplet were observed between non-isothermal and isothermal conditions.

In addition to the droplet perpendicularly impingement on a flat wall as the above literature studied, many studies have been done to study the droplet impinging on an inclined wall. Šikalo et al. [14] performed experimental study on drop impacts onto dry walls and liquid films at low impact angles and low normal *We*. They found that the low viscous liquid (water) either rebounded or deposited on smooth or wetted surfaces, while the high viscous liquid (glycerin) may also disjoin into two droplets, depending upon the impact angle. Jin et al. [15] studied the impact process of a water droplet on a cold surface with different inclined angles. It was found

that the inclined angle of the surface has a significant influence on the spreading time and displacements of the foremost and rearmost points during water droplet impact process.

Moreover, surface temperature and *We* for various single component liquids has been investigated in recent studies to segregate the post-impact outcomes on regimes maps [16-18]. Based on the heat transfer and the temperature conditions, the boiling regimes of liquid are identified as following: 1) film evaporation for T_w (wall temperature) < T_{BP} (boiling point temperature); 2) nucleate boiling for $T_{BP} < T_w < T_L$ (Leidenfrost temperature); 3) film boiling for $T_W > T_L$. Recently, quantification of temporal variation of dimensionless spreading length and contact angle have been studied experimentally under isothermal conditions [19, 20]. Nonetheless, the droplet-wall interaction phenomena under non-isothermal (different temperature for the droplet and the wall) conditions are more complicated due to the presence of the transient heat transfer, possible evaporation and variation in thermophysical properties. When $T_W < T_{BP}$, the heat transfer does not affect the droplet impact process in earlier stage of the impingement, however, does affect the spreading process due to the modification in thermophysical properties (i.e. surface tension and viscosity) [21]. In order to investigate the influence of the wall temperature on droplet extentions, a dimensionless temperature T^* is introduced as $T^*=(T_w-T_s)/(T_L-T_s)$, in which T_w, T_s and T_L are the wall temperature, saturation temperature of the liquid and Leidenfrost temperature, respectively. $T^* < 0$ indicates a cold impingement situation, while $T^* > 1$ is characterized as the Leidenfrost regime which represents the presence of the vapor layer formed at the liquid-wall interface, rendering a rapid decline of the heat transfer. By introducing the dimensionless Mundo number, $K=WeOh^{-0.4}$ [22]with T^* and combining the results of studies of Dewitte [23] and Cossali et.al [24], Labergue et al. [25] defined empirically three impingement regimes: rebound, splashing, and deposition on a $K - T^*$

diagram for a single droplet impinging on a wall (Figure 16).A number of analytical and numerical models have also been developed to help further understand the droplet-wall impingement dynamics and characteristics. Krasovitski and Marmur [26] performed a theoretical study of limiting contact angle and the hysteresis range when drops down on a tilted plate. Their results showed that the contact angles at the upper and lower contact line do not always equal the retraction and advancing contact angles, respectively. They also found that the limiting inclination angle cannot be calculated from the conventional equation based only on the advancing and retraction contact angles. In Yonemoto and Kunugi's work [27], an analytical model was developed based on energy conservation to study the dynamic process of droplet perpendicularly impingement on a solid surface. They validated the theory against the available experimental data at a wide range of *We* and found that their model can accurately predict the impinging behavior of several different liquid fuels on various solid surfaces. They derived the equations to provide the correlations between the dimensionless maximum spreading diameter and *We* or *Re* in the capillary and viscous regions. Recently, Zhao et al. [4] characterized the single fuel droplet impinging on the plate using volume of fluid (VOF) approach to better understand of the dynamic impingement process. The simulation results of the dimensionless spreading length, height ratio, and the contact angle show good agreement with the experimental results. The results also showed that the vortex is visible on the top of droplet rim during the initial spreading phase, which changes the direction when the retraction phase initiates.

The literature review presented above focus on either low viscous droplet (e.g. water) or droplet impingement on a non-inclined solid surface. However, few works investigate the high viscous droplet impinged on an inclined wall. The effect of various droplet - wall temperature conditions on the spreading stage after droplet impingement is rarely discussed as well. Therefore, in this

study, an analytical model based on energy conservation equation of a single diesel droplet impinging on the wall is developed in terms of β_m (dimensionless maximum spreading length, the ratio of maximum spreading length to initial droplet diameter) to understand the detailed impinging dynamic process. The model firstly considers a single diesel droplet impinging on the wall with different inclined angles (α); then the improved model is investigated by considering the heat energy due to droplet and wall temperature variation when inclined angle of the wall is 0°. This analytical model is verified by experiment results and is used to predict the relationship between maximum spreading length and fuel properties at different droplet – wall temperature, then also further utilized to determine the transition from capillary regime to viscous regime at different inclined wall. Moreover, the effects of liquid types and droplet size on β_m are also discussed. The paper is organized as follows: after introduction, the energy conservation based analytical model is developed. This is followed by the experimental setup and the method of data processing. Then, the results based upon the developed model are discussed. Finally, a summary of the insights is provided in conclusion.

2. Energy-budget Theory of Droplet Impinging on a Wall

2.1 A Single Droplet Impinging on an Inclined Wall

When a droplet impinges on an inclined wall, it will go through five stages: the kinetic stage, the spreading stage, the sliding stage, the retraction stage, and the stable wetting stage [3, 28]. A quantitative evaluation of heat transfer between liquid film and solid wall caused by droplet-wall interaction is important. The liquid film is widely described by the maximum spreading length. Based on the studies, the kinetic stage lasts very short (10^{-6} ms) [29, 30], which can be neglected. For spreading stage, the droplet will spread along the wall to reach its maximum spreading length. While for retraction and sliding stages, the length of liquid film will fluctuate based upon the maximum spreading length due to the complex energy transmission of the droplet interaction with the wall. Hence, in the present study, the maximum spreading length of the droplet impinged on the wall is considered.

Based on energy conservation approach [31, 32], the initial kinetic, gravitational, and surface energies prior to droplet impingement are converted into adhesion energy, viscous dissipation, deformation energy, and gravitational potential energy after impingement. Among them, the fact that adhesion forces act not only in the horizontal but also in the vertical direction at the contact line with respect to the wall has been emphasized recently [27]. Therefore, the contribution of adhesion forces in both horizontal and vertical directions must be considered. A theoretical equation expressing β_m (maximum spreading length of the droplet on the wall in terms of initial droplet diameter) as a function of contact angle of trailing edge (θ_b), inclined angle of the wall (α), *We*, and *Re* is finally derived.

E_{kine}, E_{grav}, and E_{surf} are characterized as the kinetic energy, initial gravitational potential energy, and initial surface energy of the droplet before impingement, respectively; while E_{adh}, E_{vis}, E_{def}, and $E_{grav,i}$ indicate adhesion energy, viscous dissipation, deformation energy, and gravitational potential energy at the end of spreading stage after impingement, respectively. Therefore, the energy conservation is given below:

$$E_{kine} + E_{grav} + E_{surf} = E_{adh} + E_{vis} + E_{def} + E_{grav,i} \quad (1)$$

A simplified model has been developed to show the initial energy of diesel droplet during the kinetic stage of impingement. Figure 1(a) provides the schematic of a single droplet just prior to impingement on the inclined wall with the velocity (u) in the direction of gravity. Thus, the impact velocity of the droplet is defined by $u_{imp} = u \cdot cos\alpha$. At this moment, the droplet merely touches the wall without any energy transmission or interaction with the wall.

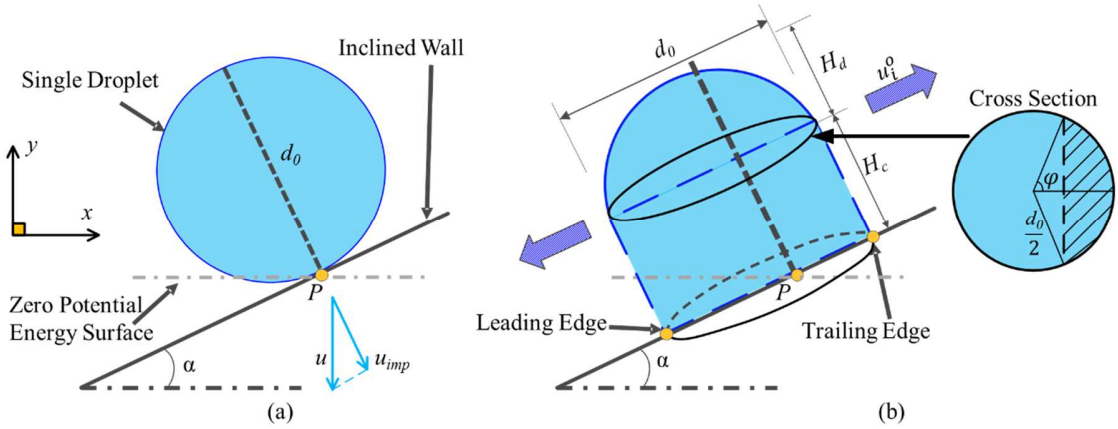

Figure 1. A schematic of single droplet impingement on an inclined wall during kinetic stage: (a) a single droplet just prior to impingement with the impact velocity (u), and (b) an assumed droplet shape with a spreading length, d_o.

A Cartesian coordinate is established, in which, the positive y direction is opposite to the gravity, while x direction is perpendicular to the y axis. The impinging point (P) that the zero potential energy surface passes through, initial droplet diameter (d_o) and inclined angle of the wall (α)

between the slope of the wall and the horizontal plane are also shown in Figure 1(a). Thus, each term on the left side of Equation (1) can be expressed as follows:

$$E_{kine} = \frac{1}{2}\rho V_o u^2 \tag{2}$$

$$E_{grav} = \frac{1}{2} d_o cos\alpha \cdot \rho g V_o \tag{3}$$

$$E_{surf} = \pi d_o^2 \sigma_{lg} \tag{4}$$

where ρ, g, V_o, σ_{lg}, and u are the density of diesel droplet, gravity acceleration, initial droplet volume, surface energy density of diesel, and droplet velocity, respectively. Additionally, in Equation (3), the expression, $\frac{1}{2} d_o cos\alpha$, indicated the distance from the centroid of droplet to the zero potential energy surface.

At droplet impingent, it is very challenge to derive the exact expressions of the energy terms on the right side of Equation (1) since E_{vis}, E_{adh}, and E_{def} highly depend on the dynamic parameters of droplet deformation such as the height of the liquid film, contact angle, spreading length and so on. Therefore, an assumed shape of the droplet with a spreading length, d_0 at the moment of impingement is suggested, as shown in Figure 1(b). The shape of the droplet includes a dome-shaped cap with a cylinder base to delineate the shape of the droplet during the initial impingement. For the dome and cylinder in this shape, each of them accounts for half of the total mass of the droplet. Equivalent height of the dome H_d and cylinder H_c are calculated as $\frac{1}{2} d_o$ and $\frac{1}{3} d_o$, respectively. Starting from this moment, the droplet starts spreading along the wall with an initial mean velocity (u_i^o). The density is assumed to be evenly distributed inside droplet. In

Figure 1(b), the dashed line that goes through point P, perpendicular to the wall divides the droplet into two parts. One is the back side (volume, V_b) moving upward with a trailing edge with respect to the impinging point; the other one is the front side (volume, V_f) moving downward with a leading edge. From the relative position relation between the center of the droplet mass and impinging point P, the distance from leading edge to point P and distance from point P to trailing edge are calculated as $\frac{tan\alpha+3}{6}d_o$ and $\frac{3-tan\alpha}{6}d_o$, respectively. Then considering the cross section of dome-cylinder shaped droplet in Figure 1(b). In cross section sketch, the area of the shaded part is the taken as the base area of the back side, which is expressed in Equation (5). In this method, the volume fraction of back side and front side with respect to the total droplet volume are calculated in Equation (6) and (7), respectively. Note that the volume of front side is larger than that of back side due to gravitational effect,

$$A_b=\left(\frac{\varphi}{180^\circ}\cdot\frac{1}{4}\pi-\frac{tan\alpha sin\varphi}{12}\right)d_o^2 \tag{5}$$

$$\frac{V_b}{V_o}=\frac{\varphi}{360^\circ}-\frac{sin2\varphi}{\pi}+\frac{54-27tan\alpha+tan^3\alpha}{648} \tag{6}$$

$$\frac{V_f}{V_o}=1-\left(\frac{\varphi}{360^\circ}-\frac{sin2\varphi}{\pi}+\frac{54-27tan\alpha+tan^3\alpha}{648}\right) \tag{7}$$

where the subscripts b and f represent the back and front side of the droplet, respectively. φ which equals to $cos^{-1}\left(\frac{tan\alpha}{3}\right)$ is the corresponding angle of the bow-shaped segment of the circle in the cross section of the cylinder. According to mass conservation, the mass of droplet flow into the control volume through cross section (round shape) in the direction normal to the wall equals

to the mass flow out through the side surface of the volume. u_i^0 is calculated from the equation below:

$$\frac{\pi}{4} d_o^2 \rho u_{imp} = \rho u_i^o \cdot \left(\frac{\pi d_o^2}{2} + \pi d_o H_c \right) \tag{8}$$

Thus, $u_i^0 = \frac{3}{10} u cos\alpha$ is obtained. The schematic to describe the movement of a diesel droplet at the spreading stage is shown in Figure 2. During the spreading stage, the droplet gradually deforms along the wall as spreading proceeds. The back side of the droplet moves upward along the negative x direction and a maximum spreading length $r_{b,m}$ is acquired when its velocity reaches zero. Then the back side of the droplet begins retraction; while the front side of droplet keeps moving along the positive x direction to the end of the spreading stage, as is shown in Figure 2. The end of spreading stages when maximum spreading length is obtained is defined as following: deformation of the droplet along the wall is completed; the curvature of the droplet surface reaches zero. At this moment, the shape of the droplet is assumed to be geometrically symmetry r_m and s_m are denoted as the distance from geometric axis to the leading edge and the displacement of geometric axis from the impinging point along the x direction, respectively. Hence, the relationship among them can be written as $r_m = r_{b,m} + s_m$. Moreover, the contact angle on leading edge and trailing edge (θ_f and θ_b, respectively) are defined as the angle formed at liquid-gas interface and solid-liquid interface at the three-phase contact point.

Thus, β_m can be calculated by the following equation:

$$\beta_m = \frac{2r_m}{d_o} = \frac{2(r_{b,m} + s_m)}{d_o} = \frac{r_{b,m} + s_m + r_m}{d_o} \tag{9}$$

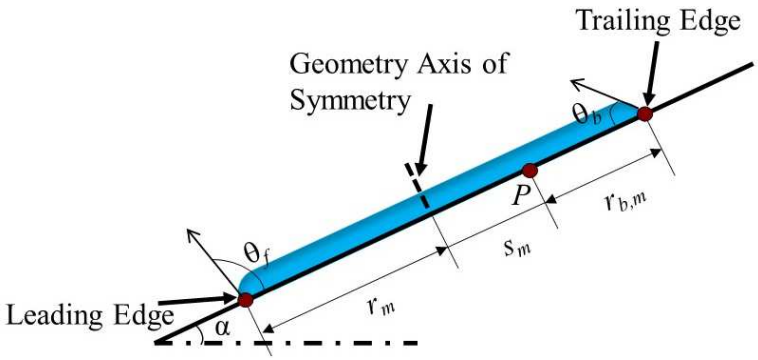

Figure 2. A schematic of single droplet after impingement on an inclined wall at the end of spreading stage.

In addition, it is perplexing to attain the exact expression of the distance from geometric axis to the leading edge as the velocity of front side keeps changing dynamically. As a consequence, only s_m and $r_{b,m}$ are studied for the maximum spreading length calculation to procure the exact expression of β_m. At the end of spreading stage, the mass of the back and front side of the droplet is evenly distributed along the wall with a certain height. Based on the volume fraction of front side of the droplet by Equation (7), s_m and $r_{b,m}$ are derived as

$$s_m = \frac{2\pi r_o^3 \tan\alpha}{3h_m r_m}\left(\frac{1}{8} + \frac{\sin\varphi}{6\pi} - \frac{\tan^2\alpha}{216}\right) \tag{10}$$

$$r_{b,m} = r_m - \frac{2\pi r_o^3 \tan\alpha}{3h_m r_m}\left(\frac{1}{8} + \frac{\sin\varphi}{6\pi} - \frac{\tan^2\alpha}{216}\right) \tag{11}$$

where h_m and r_o are the height of the liquid film at the end of the spreading stage and the initial droplet radius, respectively. In order to simplify the equation structure, the term $\left(\frac{1}{8} + \frac{\sin\varphi}{6\pi} - \frac{\tan^2\alpha}{216}\right)$ in Equation (10) and (11) is represented as symbol, *Z*.

From an energy conservation standpoint, based on the assumption above, the energies of back side of the droplet is studied. In addition, adhesion force in *y* direction must be considered, so for the back side of the droplet, each energy term in Equation (1) is derived as shown in Table 1.

In Table 1, $t_{b,m}$ is the time when $r_{b,m}$ is acquired. h_{eff} is the effective height in the liquid film which implies a distance from the wall in y axis and also indicates the height where maximum velocity of spreading is achieved. u_i is the mean velocity at the effective height along the spreading stage after droplet impingement. V_b is the volume of the back side of the droplet, determined by $V_b=m_b/\rho$. In the expression of E_{adh}, the first and second terms correspond to the adhesion energy in x and y directions at the contact line, respectively. $\overline{\theta}_b$ is adopted as the averaged contact angle of the back side when β_m is obtained under higher and lower We without splashing. In the expression of E_{def}, S_{def} refers to the deformed surface area, and it is defined as the spherical cap area (S_{cap}) of the droplet on the wall, given as

$$S_{def}=S_{cap}=\frac{\pi}{2}\left(r_{b,m}^2+h_m^2\right) \tag{12}$$

Table 1. Expression of each energy term in Equation (1) when considering the back side of the droplet.

Energy prior to impingement	Expression	Energy at the end of spreading stage	Expression
E_{kine}	$\frac{V_b}{V_o}\cdot\rho V_o u^2$	E_{adh}	$\frac{\pi}{2}r_{b,m}^2\sigma_{lg}\left(1-cos\overline{\theta}_b\right)-\left(\frac{\pi}{2}r_{b,m}h_m+h_m r_{b,m}\right)\sigma_{lg}sin\overline{\theta}_b$
E_{grav}	$\frac{V_b}{V_o}\cdot\rho g V_0 d_o cos\alpha$	E_{vis}	$\mu\left(\frac{u_i}{h_{eff}}\right)^2 V_b t_{b,m}$
E_{surf}	$\frac{V_b}{V_o}\cdot\pi d_o^2\sigma_{lg}$	E_{def}	$S_{def}\sigma_{lg}$
		$E_{grav,i}$	$m_b g\cdot\left[\left(\frac{r_{b,m}}{2}-\frac{h_m}{2}tan\alpha\right)sin\alpha+\frac{h_m}{2cos\alpha}\right]$

With the liquid film proceeding, the initial velocity (u_i^o) as described in Figure 1(b) varies according to the substantial change of the viscous force in x direction. Nevertheless, the treatment of the dissipation term (E_{vis}) in Table 1 is very complex in this sort of energy-budget approach because the precise velocity profile is hardly procured during the spreading stage.

Thus, the radical mean liquid velocity along the solid wall (u_i) is adopted to evaluate the viscous dissipation. As mentioned above, it is obvious that the initial spreading velocity of back side of the droplet after impingement decreases from $u_i^{o,max}$ at the moment in Figure 1(b) to zero at the moment in Figure 2 before it reaches its maximum spreading length. Assuming that u_i^0 equals to the mean velocity of the droplet internal velocity profile, the maximum initial velocity satisfies the condition of $u_i^{o,max} \approx 2u_i^o$, the following equation is obtained

$$u_i^{o,max} = 2u_i^o = \frac{3}{5} u\cos\alpha \tag{13}$$

Then again, because it is very challenging to determine the exact function of velocity decreasing from $u_i^{o,max}$ to zero, we assume that $u_i^{o,max}$ linearly declines with respect to the spreading length. Consequently, u_i can be calculated as $3u\cos\alpha/10$. Moreover, $t_{b,m}$ represents the time when the kinetic energy E_{kine} of the back side of the droplet is completely converted into the adhesion energy E_{adh}, and the viscous dissipation E_{vis}. Therefore, $t_{b,m}$ is given by $t_{b,m} = r_{b,m}/u$.

When the droplet impinges on an inclined wall, the droplet initially spreads and forms a lamella bounded by a thicker rim on the wall due to the recoil force from the solid surface [33]. Then the back side is pushed upward by surface tension to reach its maximum spreading length. This situation is similar to a wall jet flow, and consequently, a wall jet velocity profile [34, 35] is assumed in this study for evaluating the viscous dissipation term.

The wall jet velocity in the liquid film against to the wall provides a non-linear profile and its maximum velocity is located at a certain height above the wall. From the previous study on the wall jet [30], the peak velocity is located at around 1/4 of the effective height of the wall jet.

Therefore, the effective height of liquid film in term E_{vis} is assumed to be $h_{eff}=h_m/4$. Thus, the viscous dissipation term in Table 1 can be written as follows:

$$E_{vis}=\mu\frac{36}{25}\cdot\frac{ur_{b,m}}{h_m^2}\cdot V_b \tag{14}$$

Eventually, by substituting Equations (6), (9) to (12), (14), Table 1, $We=\rho u^2 d_o/\sigma_{lg}$, $Re=ud_o/\nu$, $Oh=\sqrt{We}/Re$, and $r_m=r_{b,m}+s_m$ into Equation (1), the following equation is derived:

$$\left(\frac{\varphi}{360^\circ}-\frac{sin2\varphi}{\pi}+\frac{54-27\tan\alpha+\tan^3\alpha}{648}\right)\cdot\left\{\frac{W_e}{3}+\frac{4r_o^2\rho g\cos\alpha}{3\sigma_{lg}}-\frac{4r_o\rho g}{3\sigma_{lg}}\left[\left(\frac{\beta_m r_o}{2}-\frac{\pi r_o^2 Z\cdot\tan\alpha}{3h_m\beta_m}-\frac{h_m}{2}\tan\alpha\right)\sin\alpha+\frac{h_m}{2\cos\alpha}\right]+4-\frac{96r_o^2\cos^2\alpha}{25h_m^2}W_e^{\frac{1}{2}}Oh\cdot\left(\frac{\beta_m}{2}-\frac{\pi r_o Z\cdot\tan\alpha}{3h_m\beta_m}\right)\right\}-\left[2\left(1-\cos\bar{\theta}_b\right)\left(\frac{\beta_m}{2}-\frac{\pi r_o Z\cdot\tan\alpha}{3h_m\beta_m}\right)^2-\frac{(2+\pi)h_m}{\pi r_o}\cdot\left(\frac{\beta_m}{2}-\frac{\pi r_o Z\cdot\tan\alpha}{3h_m\beta_m}\right)\sin\bar{\theta}_b\right]-\frac{S_{def}}{\pi r_o^2}=0 \tag{15}$$

in which, $Z=\frac{1}{8}+\frac{\sin\varphi}{6\pi}-\frac{\tan^2\alpha}{216}$ as mentioned above, h_m is calculated as follows according to [27],

$$h_m=\frac{2Af}{1+\frac{\pi}{A^2}f\beta_m^2}r_o \tag{16}$$

$$f=\sqrt[3]{\frac{3}{\pi}+\sqrt{\left(\frac{3}{\pi}\right)^2+\left(\frac{\beta_m}{A}\right)^6}}+\sqrt[3]{\frac{3}{\pi}-\sqrt{\left(\frac{3}{\pi}\right)^2+\left(\frac{\beta_m}{A}\right)^6}} \tag{17}$$

$$A=\left(\frac{4\pi}{3}\right)^{1/3} \tag{18}$$

From Equation (15), a model of droplet impinging on an inclined wall is established to reveal the relationship between β_m and *We* is acquired for a given liquid type. The energies in Equation (15) are represented in non-dimensional pattern, which are kinetic energy [$\left(\frac{\varphi}{360°} - \frac{sin2\varphi}{\pi} + \frac{54-27\tan\alpha+\tan^3\alpha}{648}\right)\cdot\frac{We}{3}$], gravitational potential energy [$\left(\frac{\varphi}{360°} - \frac{sin2\varphi}{\pi} + \frac{54-27\tan\alpha+\tan^3\alpha}{648}\right)\cdot\left\{\frac{4r_o^2\rho g\cos\alpha}{3\sigma_{lg}} - \frac{4r_o\rho g}{3\sigma_{lg}}\left[\left(\frac{\beta_m r_o}{2} - \frac{\pi r_o^2 Z\cdot\tan\alpha}{3h_m\beta_m} - \frac{h_m}{2}\tan\alpha\right)\sin\alpha + \frac{h_m}{2\cos\alpha}\right]\right\}$], viscous dissipation energy [$\left(\frac{\varphi}{360°} - \frac{sin2\varphi}{\pi} + \frac{54-27\tan\alpha+\tan^3\alpha}{648}\right)\cdot\frac{96r_o^2\cos^2\alpha}{25h_m^2}We^{\frac{1}{2}}Oh\cdot\left(\frac{\beta_m}{2} - \frac{\pi r_o Z\cdot\tan\alpha}{3h_m\beta_m}\right)$], adhesion energy [$2(1-\cos\overline{\theta_b})(\frac{\beta_m}{2} - \frac{2\pi r_o\tan\alpha}{9h_m\beta_m})^2 - \frac{(2+\pi)h_m}{\pi r_o}\cdot(\frac{\beta_m}{2} - \frac{\pi r_o Z\cdot\tan\alpha}{3h_m\beta_m})\sin\overline{\theta_b}$], deformation energy [$\frac{S_{def}}{\pi r_o^2}$], and initial surface energy [$\left(\frac{\varphi}{360°} - \frac{sin2\varphi}{\pi} + \frac{54-27\tan\alpha+\tan^3\alpha}{648}\right)\cdot 4$], respectively.

2.2 Heat Energy Consideration under Non-isothermal Condition

Considering the situation that a single droplet and the wall possess different temperature, due to the movement of the liquid, typical convective heat transfer regarding the droplet on a flat wall will happen. The process of droplet impingement under non-isothermal conditions can be described as the movement of fluid over solid surface. The transfer of heat in this condition can also be depicted as forced convection dominated heat transfer. The temporal temperature profile in droplet is perplexing to be obtained. Also, the time period during the spreading stage is quite short. Thus, the heat transfer from droplet to ambient gas due to film evaporation is assumed to be negligible. The temperature is also assumed to be uniformly distributed inside the droplet without any temperature gradient during the spreading stage. As a consequence, the heat is transferred only from the solid to liquid without extra heat loss. The relationship for heat transfer by convection is expressed as:

$$q=cS_b(T_w-T_d) \tag{19}$$

where q is the heat transferred per unit time, c is the heat transfer coefficient, S_b is the real-time contact area between the back side of the droplet and wall during the spreading stage which is expressed as $S_b=\frac{1}{2}\pi r_b^2$, where r_b is the spreading length of the back side.T_w is the initial temperature of the wall [K] and T_d is the initial temperature of the droplet [K]. As mentioned above, droplet - wall impingement is similar to a wall jet flow. In order to get the heat transfer coefficient of diesel fuel, a correlation of heat transfer coefficient and fuel properties for the impinging spray on the wall is employed which was formulated by Chang [36] as the following form:

$$Nu=0.34\frac{We^{0.94}}{Re^{0.53}Pr^{0.33}} \tag{20}$$

where Nu and Pr are the droplet Nusselt and Prandtl number, defined as $Nu = cd_o/k$, $Pr = c_p\mu/k$. In the above relationship, k is the thermal conductivity, and c_p is the specific heat at constant pressure, respectively.

Then again, recalling the mean velocity (u_i) at the effective height along the spreading stage. The total heat energy E_{heat} obtained by the back side of the droplet during the spreading stage can be derived as follows:

$$E_{heat}=c(T_w-T_d)\int_0^{\frac{r_{b,m}}{u}}\frac{1}{2}\pi(u_i t)^2 t\,dt=\frac{9\pi r_{b,m}^4}{800u^2}c(T_w-T_d) \tag{21}$$

When $T_w > T_d$, then $E_{heat} > 0$ which means the droplet absorbs the heat energy transferred from the heated wall, while if $T_w < T_d$, then $E_{heat} < 0$, so the heat energy is transferred from the droplet

to the wall. Recalling the energy conservation law of the droplet impinging on the wall, when the heat energy is considered, Equation (1) is deformed to be

$$E_{kine} + E_{grav} + E_{surf} = E_{adh} + E_{vis} + E_{def} + E_{grav,i} + E_{heat} \tag{22}$$

Then combining with Equations (15), and (19) to (22), the model that represents a single droplet impinging on a wall under non-isothermal condition is derived as:

$$\left(\frac{\varphi}{360°} - \frac{sin2\varphi}{\pi} + \frac{54-27\tan\alpha+\tan^3\alpha}{648}\right)\cdot\left\{\frac{W_e}{3} + \frac{4r_o^2\rho g\cos\alpha}{3\sigma_{lg}} - \frac{4r_o\rho g}{3\sigma_{lg}}\left[\left(\frac{\beta_m r_o}{2} - \frac{\pi r_o^2 Z\cdot\tan\alpha}{3h_m\beta_m} - \frac{h_m}{2}\tan\alpha\right)\sin\alpha + \frac{h_m}{2\cos\alpha}\right] + 4 - \frac{96r_o^2\cos^2\alpha}{25h_m^2}W_e^{\frac{1}{2}}Oh\cdot\left(\frac{\beta_m}{2} - \frac{\pi r_o Z\cdot\tan\alpha}{3h_m\beta_m}\right)\right\} - \left[2\left(1 - \cos\bar{\theta}_b\right)\left(\frac{\beta_m}{2} - \frac{\pi r_o Z\cdot\tan\alpha}{3h_m\beta_m}\right)^2 - \frac{(2+\pi)h_m}{\pi r_o}\cdot\left(\frac{\beta_m}{2} - \frac{\pi r_o Z\cdot\tan\alpha}{3h_m\beta_m}\right)\sin\bar{\theta}_b\right] - \frac{S_{def}}{\pi r_o^2} - \frac{9\rho r_0^3}{25We\sigma_{lg}^2}\left(\frac{\beta_m}{2} - \frac{\pi r_o Z\cdot\tan\alpha}{3h_m\beta_m}\right)^4 c(T_w - T_d) = 0 \tag{23}$$

similarly, the heat energy for non-isothermal conditions is presented in dimensionless pattern which is $\frac{9\rho r_0^3}{25We\sigma_{lg}^2}\left(\frac{\beta_m}{2} - \frac{\pi r_o Z\cdot\tan\alpha}{3h_m\beta_m}\right)^4 c(T_w - T_d)$.

In the later section, experimental study will be conducted to validate this model and more evaluations of the model will be presented. The theory model is validated from the results of following test conditions: single droplet impingement on an inclined wall under isothermal conditions (both droplet and wall are 25°C); single droplet impingement on a flat wall under non-isothermal conditions (heated droplet-cold wall, and cold droplet-heated wall).

3. Experiments and Data Processing

3.1 Experimental Setup and Test Conditions

The experimental setup of diesel droplet-inclined wall interaction is shown in Figure 3. It consists of a high precision syringe pump, a tilting angle vise with a smooth stainless aluminum impinging plate mounted on it, a high-speed camera, a LED source, a Fresnel lens, and a heat controller which can control the initial temperature of the droplet (output 1) and the impinging plate (output 2), respectively. The surface roughness (*Ra*) of the impinging plate is 0.8 μm. The high precision syringe has a dispensing accuracy of ±1%. When the dispensing volume and pumping rate are set, the droplet size dispensed by the syringe can be determined. It can deliver a single droplet at the rate of 0.2mL/min which is small enough to not affect the initial velocity. The time interval between consecutive droplets is enough for the high-speed camera to capture the entire impingement process of the single droplet on the dry inclined wall. From the images captured by high-speed camera, the droplet diameter is calculated via pixel-based image processing method. The droplet is released from the syringe tip when the inertial and gravitational forces overcomes the capillary forces with an initial velocity of zero, then falls down to impact the wall. Different impact velocities can be obtained by changing the distance between the syringe tip and the impinging plate. Different inclined angle of the wall can be acquired by adjusting the tilting angle vise which has a range from 0° to 90°.

The optical setup consists of an analog LED light source, and a Fresnel lens of focal length 150 mm. The horizontal distance from the Fresnel lens to the LED light source is set to be 150 mm. Therefore, the LED light rays passes through the Fresnel lens and then is converted to collimated planar light rays. The collimated planar light provides shadowgraph imaging capabilities using

the Fastcam SA 1.1 high-speed camera to capture the morphological features of the droplet-wall interaction. The high-speed camera is equipped with a 200 mm Nikon focusing lens with the shutter set F5.6 and frame speed at 24,000 frames per second. The high-speed camera is triggered after the droplet dispensed from the syringe tip. The time interval between these two triggers is slightly increased as the distance from syringe tip to the wall rises up. Thus, the camera can capture the entire droplet-wall impingement process.

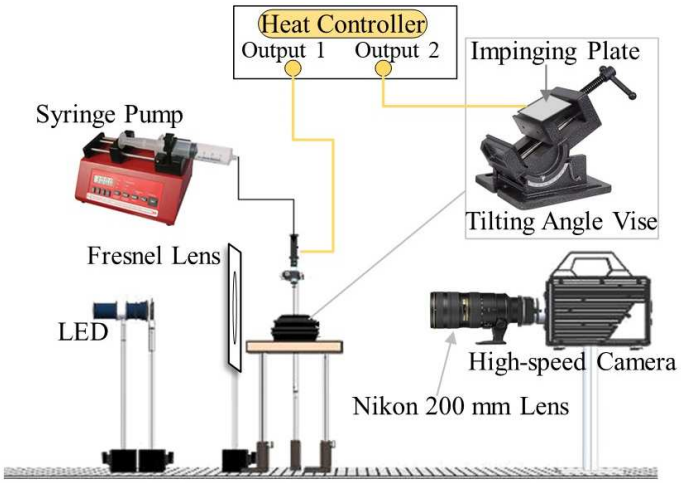

Figure 3. A schematic of experimental setup.

The control parameters in this study are: (1) the inclined angle of the wall; (2) the droplet and the flat wall temperatures; (3) the distance between the nozzle tip and the impinging point. The inclined angle is selected to be 0°, 5°, 10°, 15°, 30°, and 45°. The distance between the nozzle tip and the impinging point is set from 9 mm to 450 mm. Thus, the impact velocity ranges from around 0.4 m/s to 2.8 m/s, and the *We* ranges from around 16 to 800. It should be noted that for each test condition, the test is repeated three times to take the averaged result. The test points for temperature effect are displayed in Figure 4. The temperatures for the droplet (T_d) and the flat wall (T_w) are varied from 100℃ to 150℃ for non-isothermal conditions. The cross marker represents testing the inclined angle effect on the spreading length, while the dots are for the

non-isothermal conditions. The strategy of conducting the test is to investigate the influence of one parameter on the maximum spreading length of the droplet by controlling other parameters constant.

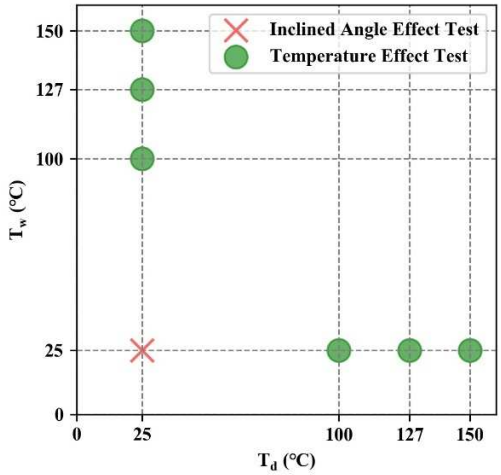

Figure 4. The map of test conditions.

3.2 Fuel Properties

The diesel fuel is employed in the current study, the thermophysical properties of diesel will change with different ambient temperature and pressure conditions. When diesel temperature increasing, the density of diesel slightly changes which is assumed to be constant, 848 Kg/ m^3. Eötvös Ramsay-Shield relation of surface tension and temperature [37] reveals a linear relationship between the surface tension (σ) and temperature. As is shown in Figure 5 [38], when temperature is inclined from 0℃ to 400℃, surface tension of diesel declines linearly. A fitted curve can be expressed as Equation (24) with the regression coefficient R^2 = 0.993. Meanwhile, the trend of kinematic viscosity (ν) can be expressed by a 6-order power function as is shown in Equation (25). The regression coefficient R^2 = 0.999.

$$\sigma = -6.60\times10^{-5}T+0.03 \quad (24)$$

$$v=6.19-1.44\times10^{-1}T+1.58\times10^{-3}T^{2}-9.11\times10^{-6}T^{3}+2.82\times10^{-8}T^{4}-4.40\times10^{-11}T^{5}+2.72\times10^{-14}T^{6} \quad (25)$$

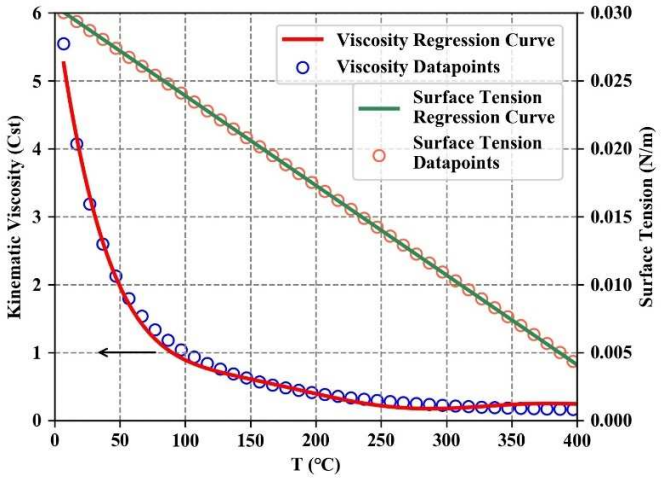

Figure 5. Diesel fuel properties change with temperature.

3.3 Data Processing

MATLAB code is implemented for experimental image processing, as is shown in Figure 6. The spreading characteristics when spreading stage ends: initial droplet diameter (d_o), impact velocity (u), contact angle (θ_b) of the back side of the droplet, and β_m of the droplet are determined. Briefly, the raw images of the droplet, extracted using Otsu's method [39] of binarization and edge detection algorithm, is used to calculate these characteristics. The initial droplet diameter (d_o), impact velocity (u) are estimated through images before the droplet impinges on the wall.

In Figure 6(a), the background was subtracted to remove the unnecessary information other than the droplet based on the original image. The possible deformation of an impacting droplet due to drag force was measured by determining the difference between horizontal and vertical diameters. The difference is less than ±1% for all measurements, showing that the drag force does not have a substantial influence on droplet size. Therefore, the image of the droplet is approximated as a circle, based on the area of this circle, the initial diameter of the droplet is

extracted. In some cases when the droplet was not completely circular the radius was calculated by averaging the distance of each pixel point on circumference with the centroid. A sensitive analysis for the threshold value was done by increasing and decreasing default threshold by 20% and the initial droplet diameter shows only ±1% for different threshold values. The initial droplet diameter is calculated and determined as 3.04 mm for the theory model from experimental results. Additionally, for each test condition, the difference of impact velocity for three test repeats is less than 2%, for example, when distance from the nozzle tip to the plate is set to be 100, the averaged impact velocity is around 1.392 m/s, *We* is still in the range of 170 to 184.

As is shown in Figure 6(b), when the droplet just impinges on the wall, the boundary of the droplet and its reflection merge together. The middle point merged line is defined as the impinging point (P). The red line indicates the inclined wall, and the blue line is the line perpendicular to the plane passing through the P point.

Figure 6(c) and (d) display how the end of spreading stage is captured in image. As is discussed before, the maximum spreading length is obtained: when the deformation of the droplet in *y* direction is completed, and the surface of droplet becomes flat along the wall. The R-squared regression model [15] is adopted. In Figure 6(c), during the spreading stage, the boundary of the droplet is composed of two parts: the cap (blue curve) and the contact area (red line). The cap is taken as the observed curve. For the blue cap, the bended boundary on both side which contact with the wall is cut off. Then the remnant is linearly fitted which is shown as a pink line. Thus, R-square is the percentage of the variance in fitted line, and when it is higher than 99.85%, the spreading stage ends, as is shown in Figure 6(d).

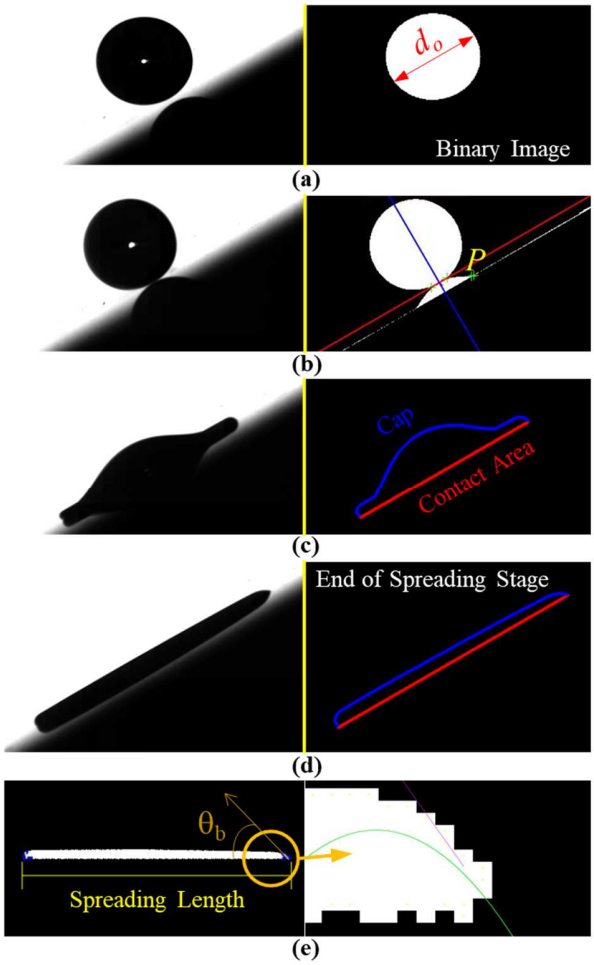

Figure 6. Image processing procedure: (a) method of calculating initial droplet diameter, (b) method of locating the inclined wall, (c) using R-square regression tool to find the end of spreading stage, (d) the end of the spreading stage, and (e) using polynomial fitting to measure the contact angle.

In order to calculate the spreading length and contact angle, the image from Figure 6(d) is rotated clockwise by the inclined angle (α), as shown in Figure 6(e). The extreme points of the droplet boundary are used to measure the maximum spreading length and contact angle of the back side of the droplet. The maximum spreading length is calculated as the distance between right and left three-phase contact points. In the meanwhile, since the boundary of each image is calculated and obtained, 20 adjacent points to the three-phase contact point are curve fitted. The order of this polynomial curve fitting is varied from 1 to 4, a curve with best fitting for the given points is acquired by comparing R-square value. Then the three-phase contact point is determined by

extrapolating the best fit curve (green solid line in Figure 6(e)) and a tangent line (purple solid line in Figure 6(e)) is drawn at this point on the curve. The angle of from this tangent to the liquid solid interface(horizontal) is considered as the contact angle [14].

4. Results and Discussions

4.1 Dynamic Phenomenon of Droplet Impingement on an Inclined Wall

All cases are non-splashing events for droplet-wall impingement. The dimensionless spreading length (β) is defined as the ratio of the droplet spreading length to the initial droplet diameter. The moment of droplet acquires a spreading length d_o is adopted as the starting point of time (t), as is shown in Figure 1(b). Also, a dimensionless time (τ) is defined by using the format tu/d_o. u is the impinging velocity, and d_o is the initial droplet diameter, respectively. When the angle of the wall is set to be 0°, both wall and droplet temperature are 25℃, Figure 7(a) shows β changing with t, while Figure 7(b) shows β changing with τ. By comparing these two figures, as impact velocity increases from u to 2.6u, from starting point, the time that the droplet takes to reach β_m also increases. As a result, τ can reflect the dynamic changes of the droplet spreading behavior more clearly.

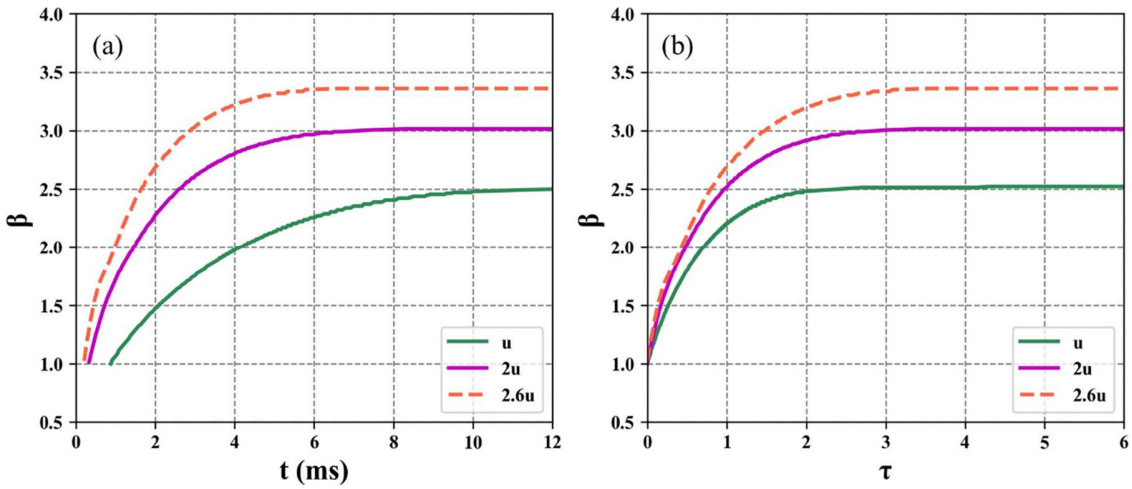

Figure 7. β changes with time at different impact velocity: (a) real time (t), and (b) dimensionless time (τ).

Figure 8 shows the experimental results of spreading movement of a droplet that initially possesses an *We* of 168 impinging on a smooth stainless Aluminum wall with an inclination of 0°, 15°, 30°, and 45°. Overall, a droplet goes through the following stages when impinges on an inclined wall: the kinetic stage, the spreading stage, the retraction and sliding stage.

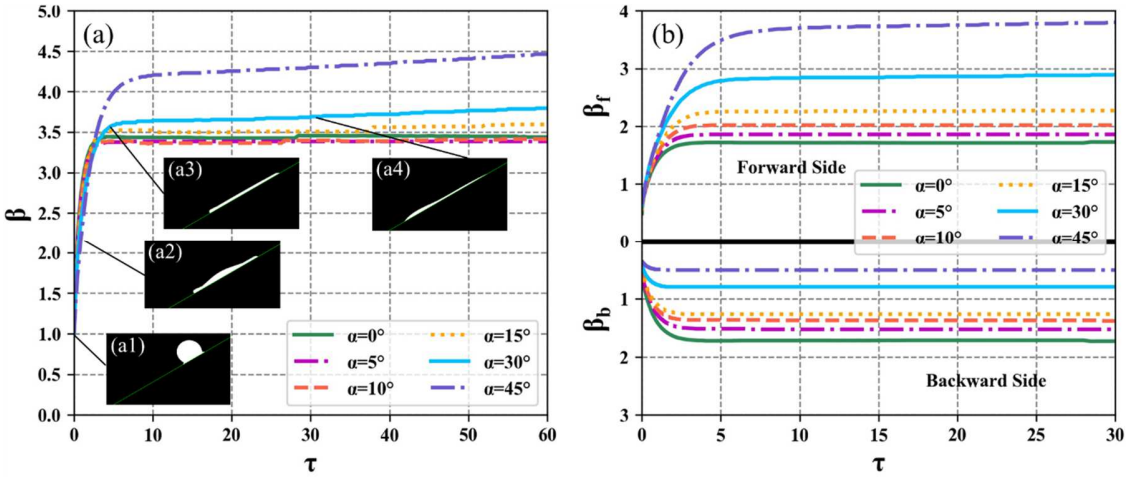

Figure 8. β of droplet changes with τ on the inclined wall with the *We* of 168 when both wall and droplet temperature are 25℃: (a) β changes with τ, and (b) β_f and β_b change with τ.

In the kinetic phase, the droplet deforms after collision, resembling a truncated sphere, at which stage the bottom of the droplet has not yet begun to spread [4]. The kinetic stage lasts very short and can be ignored in the high-speed camera of this experiment. In Figure 8(a), during the spreading stage (from (a1) to (a3) for $\alpha > 0°$), the droplet spreads immediately after the impingement, and forms a lamella bounded by a thicker rim. The initial kinetic energy of the droplet transforms into deformation energy, internal energy and kinetic energy of the fluid inside the droplet. β increases rapidly to reach its maximum, β_m, as is shown in Figure 8(a3). With the increasing of the inclination of the wall, β_m rises from around 3.3 to around 4.2, and the time it takes from (a1) to (a3) will also increase. At the retraction stage (from (a3) to (a4) for $\alpha > 0°$), β keeps almost constant when the inclined angle is set to be 0°, while due to the effect of surface tension, the upper surface of the droplet tends to contract toward geometric center. With the

augment of the inclination angle, as is shown in (a3) and (a4), β shows an obvious upward trend due to the combining effect of gravity and surface tension. The higher inclined angle, the more mass accumulates on the front side of the droplet, and thus the more gravity effect, and when it exceeds the surface tension ($\alpha > 15°$), β will increase slowly, as is shown in Figure 8(a). The sliding stage (from (a4) to the end) indicates the droplet maintains a certain shape as shown in (a4) falling down along the wall. If inclined angle is larger than 15°, β keeps increasing.

Figure 8(b) display dimensionless spreading length of front side (β_f) and back side (β_b) of the droplet changing with the dimensionless time from the start of impingement to the end of retraction stage. Obviously, $\beta_m = \beta_f + \beta_b$. It can be seen that when $\alpha = 15°$, $\beta_f = \beta_b$ which means the displacement of back side and that of front side are asymmetric along the wall. As the increasing of inclined angle, the maximum β of back side will decrease, while that of the front side will increase since much more mass of droplet is distributed on the front side.

4.2 Dynamic Phenomenon of Droplet Impingement on a Flat Wall under Non-isothermal Condition

In Figure 9, when the inclined angle of the wall is 0°, *We* of the droplet before impingement is 187, β of droplet changes with dimensionless time under non-isothermal conditions are investigated: single heated droplet impinges on cold wall (Figure 9(a)); single cold droplet impinges on heated wall (Figure 9(b)). All cases are non-splashing events for droplet-wall impingement with the same droplet impact velocity.

In Figure 9(a), the wall temperature is set to constant 25℃, and the result acquired when droplet is also 25℃ is employed as the baseline reference. When droplet is heated to higher temperature

(100, 127, and 150℃), these conditions are the similar to that occurred in the cold-start condition of internal combustion engines. For these conditions only spreading and equilibrium phases are observed, and no retraction is seen in any case. Even for these conditions β_m occurs around 3.5 (dimensionless time). Figure 9(a1) to (a4) shows the following stages: impingement, spreading, maximum spreading length, and equilibrium, respectively. as the augment of droplet temperature, β_m will also increase. This is because when droplet temperature inclines, the viscosity and surface tension of diesel fuel tends to decrease as discussed in Figure 5. Lower viscosity and surface tension will result in weaker retraction phenomenon. Meanwhile, the same conclusion can also be obtained from the Energy-budget model (Equation (23)). When viscosity and surface tension declines, β_m will increase from the calculating Equation (23).

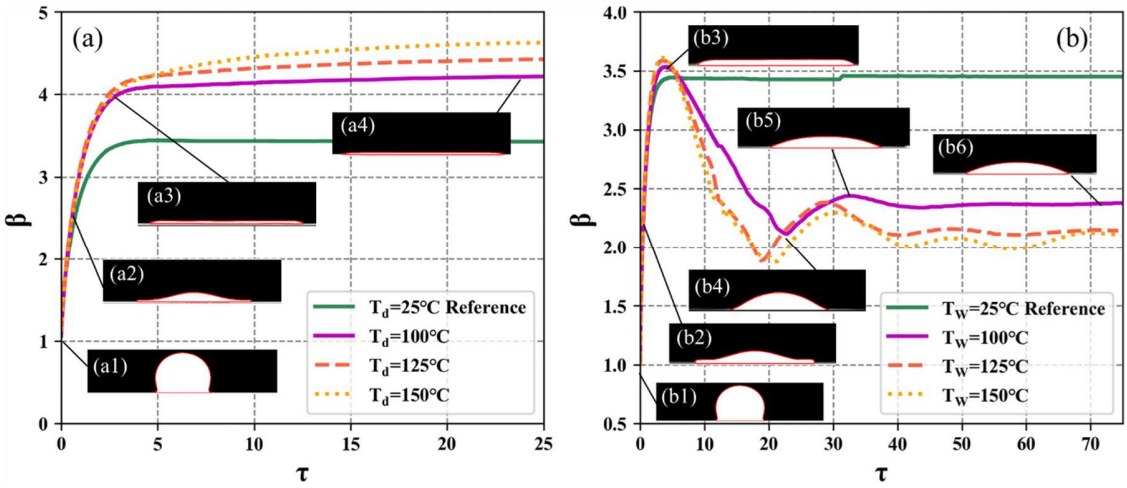

Figure 9. β changes with τ on a flat wall under non-isothermal conditions: (a) single heated droplet impinges on a cold wall, and (b) single cold droplet impinges on a heated wall.

In Figure 9(b), the droplet temperature is kept constant at 25℃, while the wall temperature is varied from 100, 125 and 150℃. When a cold droplet impacts on a heated wall, the droplet initially spreads to maximum spreading length (Figure 9(b3)) and then starts to recoil and reaches the minimum spreading length (Figure 9(b4)). Then the droplet undergoes the processes of spreading and retraction again until the kinetic energy is totally transformed to be deformation

energy and internal energy so as to acquire an equilibrium status. The process of transition from spreading to recoiling continues and the strength of recoiling depends on the temperature of the wall. β_m increases with the wall temperature rising up, but when the wall temperature exceeds 100°C, β_m almost remains constant which is approximate 3.6.

From Figure 9, a couple of important points can be made that the droplet behavior under different temperature conditions (heated droplet or heat wall) are different. Firstly, when only droplet is heated, as the droplet temperature rises up, the initial surface tension and viscosity value of droplet decreases dramatically at temperatures such as 100℃,125℃ and 150℃, as is shown in Figure 5. The inertial forces dominate over both the surface tension and viscous forces. Thus, the droplet spreads out completely in a short time period. While when the cold droplet interacts with the heated wall, the heat flux from the plate to impinged droplet causes the increase in temperature of interfacial boundary layer and hence a decline in viscosity is expected according to Figure 5. However, the overall droplet temperature is still low enough, which results in high surface tension. This may cause extensive retraction to take place. Then kinetic energy during retraction, deformation energy (surface tension determined), viscous dissipation energy (viscosity determined) and the internal energy of the droplet will be transformed mutually rendering the fluctuation of the droplet shape to reach the final equilibrium state.

4.3 Validation of Energy-budget Theory

Figure 10 illustrates the relationships among β_m and *We* for droplet impinging on an inclined wall when both droplet and wall temperature are 25°C.

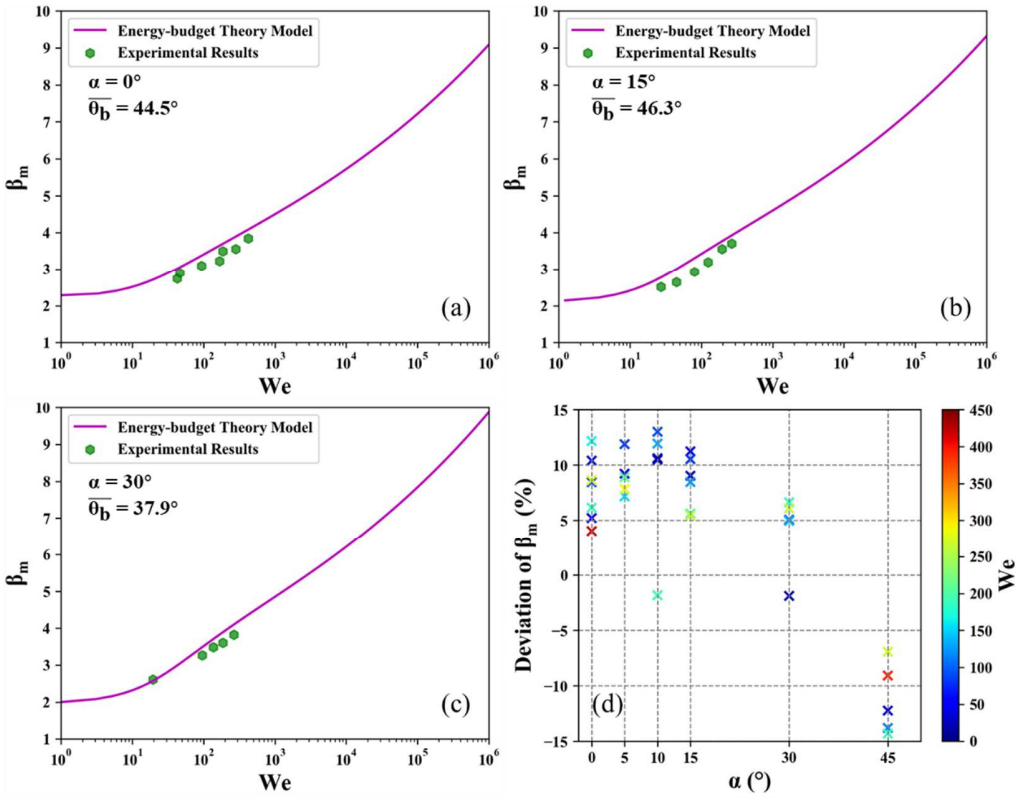

Figure 10. Relationship between β_m and *We* for diesel droplet when temperature of droplet and wall is 25°C: (a, b, and c) β_m versus *We* when α = 0°, α = 15 °, and α = 30°, respectively; (d) deviation of β_m at different inclined angle.

In each figure, $\overline{\theta_b}$ is the averaged contact angle of back side of the droplet when β_m is obtained at different *We* without splashing in the current experiments. The purple line corresponds to the limiting solutions obtained by the present theory model. The green dots represent the experimental data obtained from experimental results. In the current study, *We* ranges from approximately 33 to 420. It is obvious that with the increasing of *We*, β_m keeps rising up, and when *We* exceeds a value which is below 10, β_m increases drastically. In Figure 10(d), the deviation of β of the experimental results is defined as shown in Equation (26). The marker value represents the deviation of β, while its color indicates the corresponding *We* of the test points. The deviation of β_m for the test points are less than 15%. Thus, the current theory model can predict β_m under a limited range of *We* as is shown above.

$$\text{Deviation of } \beta_m = \frac{\text{theoretical } \beta_m - \text{experimental } \beta_m}{\text{theoretical } \beta_m} \times 100\% \quad (26)$$

Similarly, the relationships among β_m and *We* for droplet impinging on a flat wall under non-isothermal conditions are displayed in Figure 11.

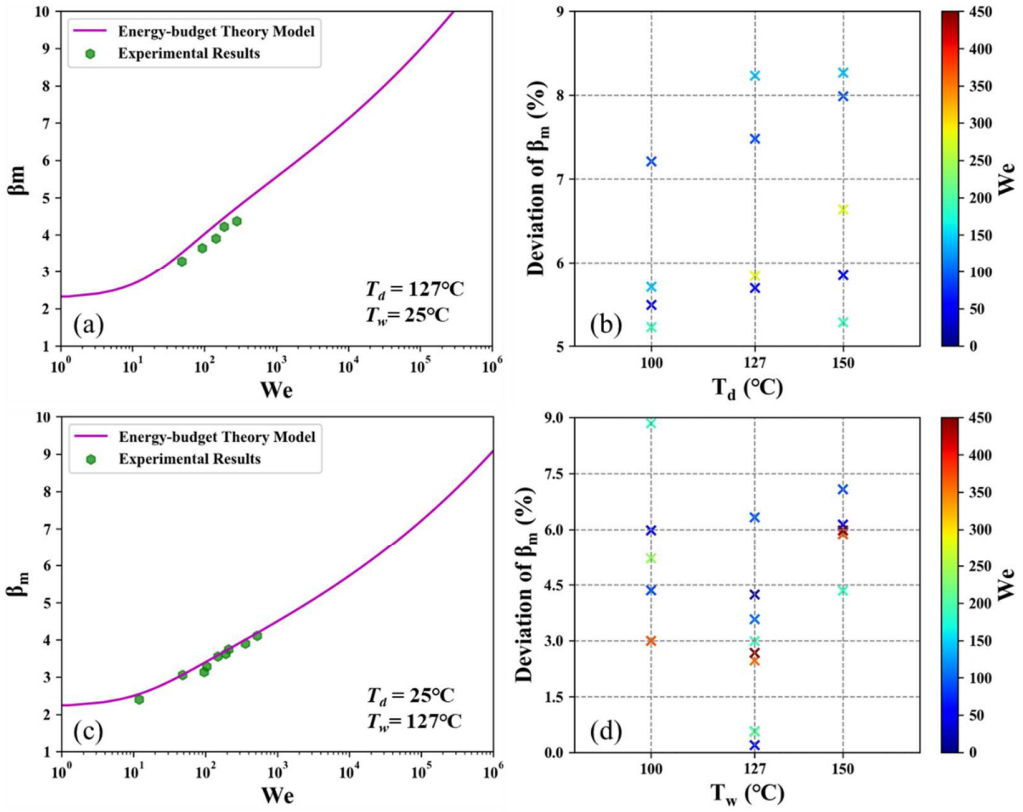

Figure 11. Relationship between β_m and *We* for diesel droplet under non-isothermal conditions: (a) β_m for heated droplet (T_d = 127°C) - cold wall (T_w = 25°C) impingement, (b) deviation of β_m at different T_d, while (c) β_m for cold droplet (T_d = 25°C) - heated wall (T_w = 127°C) impingement, and (d) deviation of βm at different T_w.

β_m shows an upward trend with the increase of the *We* for both heated droplet-cold wall and cold droplet-heated wall impingement, which can be seen from Figure 11(a) and (c), respectively. Additionally, from Figure 11(b) and (d), the deviation of β_m for the test points are less than 10%. Thus, the current theory model with heat energy consideration can be employed to predict β_m under a limited range of *We* as is shown above.

4.4 Energy Transition Analysis of Droplet Impingement on Inclined Wall

Figure 12 depicts when temperature of droplet and wall is 25℃, the non-dimensional energies changes with the changing of *We* by taking the diesel droplet impinging on a wall with the inclination of 30° as an example. As is shown below, for each dimensionless energy term listed on the left, the marker size describes the amount of energy, thus the larger radius, the more energy. Also, the marker color which corresponds to the color bar indicates the amount of energy.

The energy transition from capillary to kinetic regimes the *We* where kinetic energy exceeds deformation energy is characterized as the transition point A, which is between 10 and 100. In the region to the left of A, a capillary regime is defined for back side of the droplet when impinges on an inclined wall, where the deformation energy is comparable to the adhesion energy. In the regime between point A and point C (*We* near 1000), the kinetic energy dominates. While in the meantime, with the increase of *We*, the viscous dissipation energy exceeds adhesion energy at point B (*We* is around 100). From point B on, the viscous dissipation energy becomes more pronounced. Thus, a viscous regime is designated to the right of point C, where the effect viscous dissipation energy appears to be stronger and comparable to the kinetic energy. In viscous regime, the kinetic energy and gravitational potential energy begins to be transformed into viscous dissipation. The current test conditions are mostly located in kinetic regime where the kinetic energy dominates the spreading stage of back side of the droplet, and both kinetic energy and gravitational potential energy promote the spreading stage of the front side of the droplet.

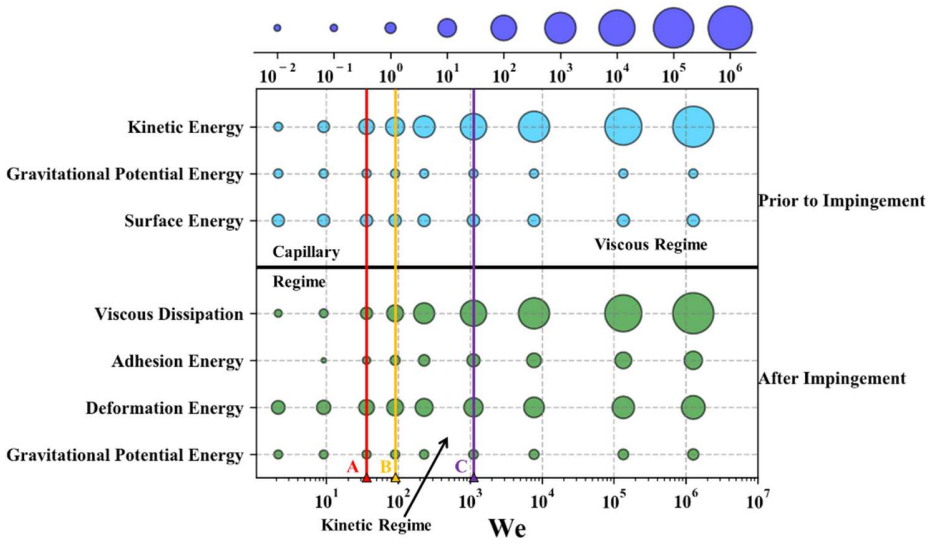

Figure 12. Non-dimensional energy transition from capillary to viscous regimes of the back side of a single droplet on an inclined wall when droplet and wall are 25℃.

4.5 Inclined Angle Effect

Figure 13 shows the effect of different inclined angle of the wall on β_m of the droplet for different *We* without splashing. When the *We* remains the same, higher than 60, as the inclined angle of the wall increases, β_m rises up gradually. When *We* is lower than 60, from Figure 11, the back side of the droplet is in the capillary regime, the inclined angle has more influence on adhesion energy than gravitational potential energy and the kinetic energy of the droplet is negligible, thus, the whole droplet is in capillary regime, where β_m has a negative correlation with the inclined angle. Consequently, as the inclined angle increases, β_m decreases. However, as *We* rises up higher, the droplet goes beyond the transition point A, and the kinetic energy and viscous dissipation energy dominate the spreading stage, so β_m rises as the inclined angle increases. The higher inclined angle, more apparent the upward tendency of β_m.

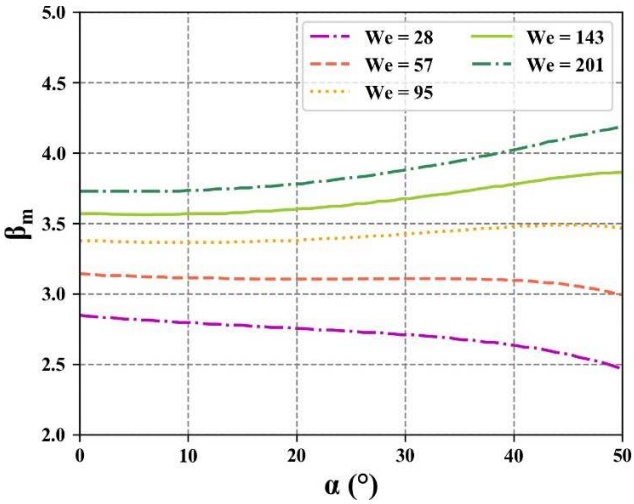

Figure 13. The effect of different α on β_m when droplet and wall are 25℃.

4.6 Fuel Properties Effect

A good correspondence with the theory is obtained for the experimental initial droplet diameter. Figure 14 shows the predicted effect of different initial droplet diameter on β_m when the inclined angle of the wall is set to be 30° for different *We* without splashing.

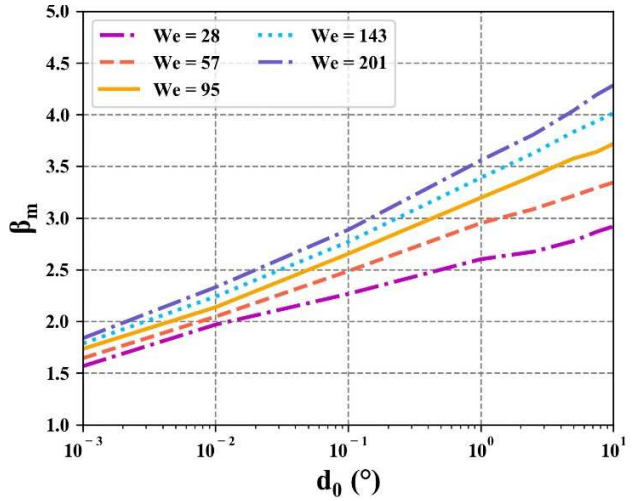

Figure 14. The effect of different d_0 on β_m when droplet and wall are 25℃.

As is shown in Figure 14, it is manifest that when the *We* is stable, as the initial droplet diameter increases from 0.001 mm to 10 mm, β_m displays a continued upward trend. This may due to that

bigger sized droplet provides more mass to the front side of the droplet and push the droplet forward along the wall. As the augment of the *We*, the slope of each line rises up. This means that when the droplet size remains constant, more kinetic energy can lead to larger spreading length.

When the inclined angle of the wall is set to be 30°, the effect of different liquid types which are diesel, purified water, N-dodecane, and N-heptane on β_m under room temperature are studied, as is shown in Figure 15. The thermophysical properties of these liquid type under room temperature (25℃) are listed in Table 2.

Table 2. The thermophysical properties of different liquid types under room temperature.

Liquid type	Density	Surface	Kinematic viscosity
	$Kg \cdot m^{-3}$	N/m	Cst
Diesel	848	0.026	2.6
Purified water	1000	0.073	1.0
N-dodecane	750	0.025	1.97
N-heptane	684	0.020	0.38

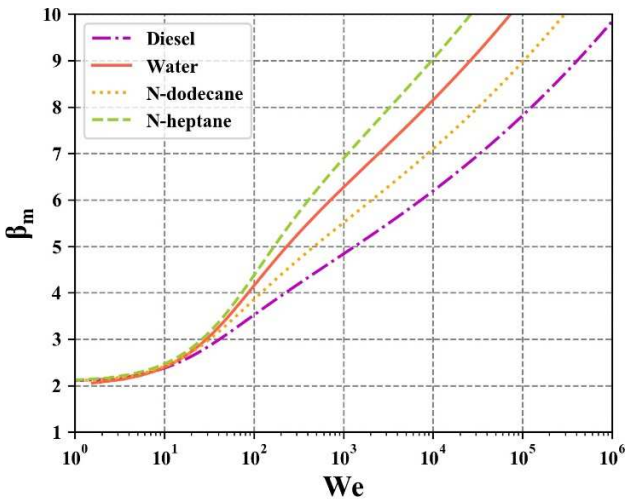

Figure 15. The effect of different liquid type on β_m when droplet and wall are 25℃.

As is shown in Figure 15, as We rises up, β_m also maintains an upward tendency for different liquid types. When *We* is lower than 20, β_m of four types of fuel are almost the same, and when We goes higher, β_m of four types of fuel can be arranged from large to small as purified water, N-heptane, N-dodecane, and diesel.

4.7 Temperature Effect

Based on the current wall temperature conditions and the corresponding *We* of non-splashing cases according to Ref. [25], the relationship between the dimensionless Mundo number (*K*) and dimensionless temperature (*T**) for current wall temperature conditions can be diagrammed in Figure 16 below. It is obviously verified that all the wall temperature conditions are located in the deposition regime.

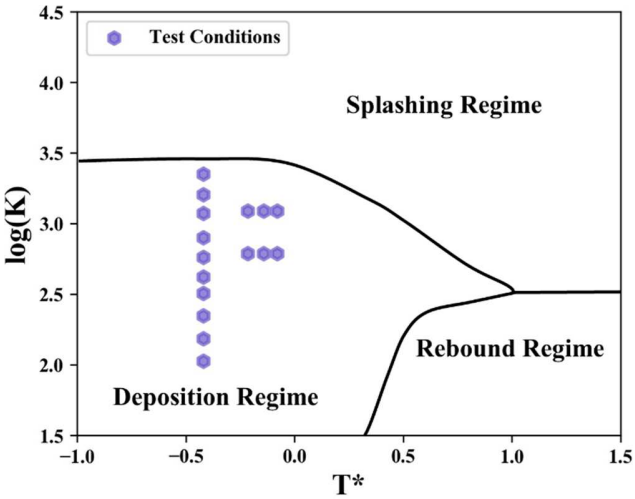

Figure 16. *K* - *T** diagram representing the boundaries between the different impact regimes [25]with current test conditions.

Figure 17 displays the temperature difference between wall (T_w) and droplet (T_d) influences on the β_m for different *We* without splashing. As is shown in Figure 17, the abscissa is defined as

temperature difference ($\Delta T = T_d - T_w$). The plot is divided into two regions: $T_d > T_w = 25$℃, and $T_w > T_d = 25$℃. Overall, with *We* rising up, the β_m also maintains an upward tendency.

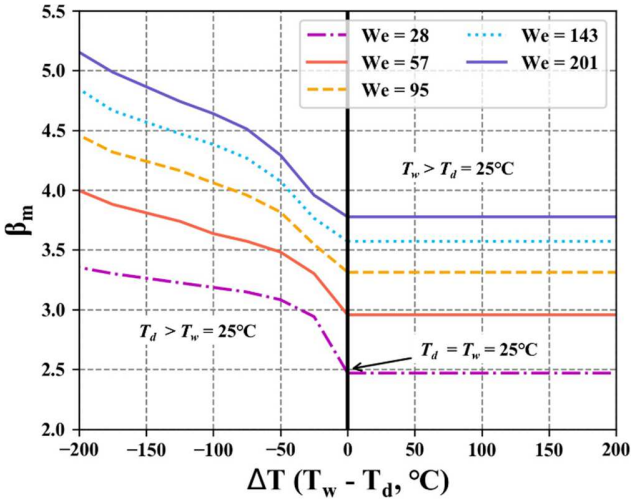

Figure 17. The effect of ΔT on β_m.

In the left region (-200℃ < ΔT < 0℃), when *We* remains the same, as the droplet temperature increases (ΔT decreases), the β_m rises up, but the growth rate gradually declines. This is because when droplet temperature is higher than 25℃, the diesel fuel properties (viscosity and surface tension) declines with temperature as is shown in Figure 5. When the droplet temperature is raised from 25℃ to 100℃, kinematic viscosity declines dramatically, while the surface tension keeps decreasing linearly. From Equation (23), lower viscosity and surface tension will result in a larger β_m. However, when droplet temperature exceeds around 100℃ (ΔT < -75℃), on the one hand, the surface tension still declines with temperature, while the viscosity of the diesel remains almost constant. Thus, the effect of thermophysical properties is weakened. On the other hand, that much more heat is released from the diesel droplet exerts a negative influence on β_m as well.

In the right region (0℃ < ΔT < 200℃), when *We* keeps constant, as the wall temperature increases (ΔT increases), β_m almost keeps constant. This is because the spreading process lasts for only a short time, thus the heat energy will not change a lot which has a small influence on β_m.

To sum up, the We which indicates the kinetic energy has large influence on βm, and the droplet temperature also influences βm due to the changes in thermophysical properties.

5. Conclusions

In this paper, an analytical energy-budget model for a single diesel droplet impinging on the wall with different α under isothermal and non-isothermal environments is developed in terms of β_m (the ratio of maximum spreading length to initial droplet diameter) to understand the detailed impinging dynamic process. Experimental study is also performed to validate the model and investigate the spreading behavior of droplet impinging on an inclined wall and of droplet impinging on a flat wall under non-isothermal conditions. The main results can be summarized as follows:

- The analytical model is validated by the experimental data at the operating points. The model is further utilized to determine the transition point between capillary regime, kinetic regime and viscous regime at a certain inclined angle of the wall based on energy-budget consideration.
- β_m increases slightly with α increasing from 0° to 45°, the time duration of the spreading stage also increases due to the effect of gravity.
- Under non-isothermal conditions, for heated droplet-cold wall impingement, β_m shows an upward trend with the droplet temperature increasing; while for cold droplet-heated wall impingement, β_m increases a bit with the wall temperature goes from 25℃ to 100℃ and then almost remains the same when wall temperature is higher than 100℃.
- As the inclined angle increases, β_m decreases. With d_0 rising up, β_m shows an upward trend. The *We* which indicates the kinetic energy has large influence on β_m, and the droplet temperature also influences β_m due to the changes in thermophysical properties of the droplet.

- Based on the wall temperature conditions in current study with corresponding test We, all test conditions are located in deposition regime. The current energy-budget model can be validated by the experimental results. This model could be further studied for the test conditions in splashing regime and rebound regime in the future.

References

1. Stanton, D. and Rutland, C., "Modeling Fuel Film Formation and Wall Interaction in Diesel Engines," SAE Technical Paper 960628, 1996, doi: 10.4271/960628.
2. Drake, M., et al., "Piston Fuel Films as a Source of Smoke and Hydrocarbon Emissions from a Wall-Controlled Spark-Ignited Direct-Injection Engine," SAE Technical Paper 2003-01-0547, 2003, doi: 10.4271/2003-01-0547.
3. Lindagren, R. and Denbratt, I., "Influence of Wall Properties on the Characteristics of a Gasoline Spray After Wall Impingement," SAE Technical Paper 2004-01-1951, 2004, doi: 10.4271/2004-01-1951.
4. Zhao, L., et al., "Splashing Criterion and Topological Features of a Single Droplet Impinging on the Flat Plate," SAE Technical Paper 2018-01-0289, 2018, doi: 10.4271/2018-01-0289.
5. Zhao, L., et al., "Characterization of Impingement Dynamics of Single Droplet Impacting on a Flat Surface," SAE Technical Paper 2019, doi: 10.4271/2019-01-0064.
6. Zhao, L., "An experimental and computational study of fuel spray interaction: fundamentals and engine applications," 2018.
7. Lee, S. and Zhao, L., "Droplet Impingement and Evaporation on a Solid Surface", in *Two-Phase Flow for Automotive and Power Generation Sectors*. 145-183, 2019, Springer, doi: 10.1007/978-981-13-3256-2_6.
8. Potham, S., Zhao, L., and Lee, S., "Numerical Study on Evaporation of Spherical Droplets Impinging on the Wall Using Volume of Fluid (VOF) Model," SAE Technical Paper 2017, doi: 10.4271/2017-01-0852.
9. Bai, C., et al., "Modeling of gasoline spray impingement," *Atomization and Sprays*. 12: 1-3, 2002, doi: 10.1615/AtomizSpr.v12.i123.10.
10. Habchi, C., et al., "Influence of the wall temperature on the mixture preparation in DI gasoline engines," *Oil & Gas Science and Technology*. 54(2): 211-222, 1999, doi: 10.2516/ogst:1999017.
11. Ohnesorge, W.v., "The formation of drops by nozzles and the breakup of liquid jets," *UT Faculty/Researcher Works*. 2019, doi: 10.26153/tsw/3391.
12. Stow, C. and Hadfield, M., "An experimental investigation of fluid flow resulting from the impact of a water drop with an unyielding dry surface," *Proceedings of the Royal Society of London. A. Mathematical Physical Sciences*. 373(1755): 419-441, 1981, doi: 10.1098/rspa.1981.0002.
13. Zhu, X., et al., "Investigation of the Effects of Heat Transfer and Thermophysical Properties on Dynamics of Droplet-Wall Interaction," SAE Technical Paper 2019-01-0296, 2019, doi: 10.4271/2019-01-0296.
14. Šikalo, Š., Tropea, C., and Ganić, E., "Impact of droplets onto inclined surfaces," *Journal of colloid interface science*. 286(2): 661-669, 2005, doi: 10.1016/j.jcis.2005.01.050.
15. Jin, Z., Zhang, H., and Yang, Z., "The impact and freezing processes of a water droplet on a cold surface with different inclined angles," *International Journal of Heat and Mass Transfer*. 103: 886-893, 2016, doi: 10.1016/j.ijheatmasstransfer.2016.08.012.
16. Tang, C., et al., "Dynamics of internal jets in the merging of two droplets of unequal sizes," *Journal of Fluid Mechanics*. 795: 671-689, 2016, doi: 10.1017/jfm.2016.218.

17. Bertola, V., "An impact regime map for water drops impacting on heated surfaces," *International Journal of Heat and Mass Transfer*. 85: 430-437, 2015, doi: 10.1016/j.ijheatmasstransfer.2015.01.084.
18. Liang, G., et al., "Boiling from liquid drops impact on a heated wall," *International Journal of Heat and Mass Transfer*. 100: 48-57, 2016, doi: 10.1016/j.ijheatmasstransfer.2016.04.061.
19. Roisman, I., et al., "Drop impact onto a dry surface: Role of the dynamic contact angle," *Colloids Surfaces A: Physicochemical Engineering Aspects*. 322(1-3): 183-191, 2008, doi: 10.1016/j.colsurfa.2008.03.005.
20. Yokoi, K., et al., "Numerical studies of the influence of the dynamic contact angle on a droplet impacting on a dry surface," *Physics of Fluids*. 21(7): 072102, 2009, doi: 10.1063/1.3158468.
21. Healy, W.M., Hartley, J., and Abdel-Khalik, S., "On the validity of the adiabatic spreading assumption in droplet impact cooling," *International Journal of Heat Mass Transfer*. 44(20): 3869-3881, 2001, doi: 10.1016/S0017-9310(01)00041-2.
22. Mundo, C., Sommerfeld, M., and Tropea, C., "Experimental studies of the deposition and splashing of small liquid droplets impinging on a flat surface," *ICLASS-94 Rouen, France*. 1994.
23. Dewitte, J., Berthoumieu, P., and Lavergne, G. *An experimental study of droplet–hot wall interactions and a survey of the splashing regime*. in *5th International Symposium on Multiphase Flow, Heat Mass Transfer and Energy Conversion, ISMF*. 2005.
24. Cossali, G.E., Marengo, M., and Santini, M., "Single-drop empirical models for spray impact on solid walls: a review," *Atomization and Sprays*. 15(6), 2005, doi: 10.1615/AtomizSpr.v15.i6.50.
25. Labergue, A., Gradeck, M., and Lemoine, F., "Experimental investigation of spray impingement hydrodynamic on a hot surface at high flow rates using phase Doppler analysis and infrared thermography," *International Journal of Heat and Mass Transfer*. 100: 65-78, 2016, doi: 10.1016/j.ijheatmasstransfer.2016.01.041.
26. Krasovitski, B. and Marmur, A., "Drops down the hill: theoretical study of limiting contact angles and the hysteresis range on a tilted plate," *Langmuir*. 21(9): 3881-3885, 2005, doi: 10.1021/acs.langmuir.8b03604.
27. Yonemoto, Y. and Kunugi, T., "Analytical consideration of liquid droplet impingement on solid surfaces," *Scientific reports*. 7(1): 2362, 2017, doi: 10.1038/s41598-017-02450-4.
28. Zhao, L., et al., "Investigation of Multi-Hole Impinging Jet High Pressure Spray Characteristics under Gasoline Engine-Like Conditions," SAE Technical Paper 2016-01-0847, 2016, doi: 10.4271/2016-01-0847.
29. Saito, A. and Kawamura, K., "Behavior of fuel film on a wall at fuel spray impinging," *International Journal of Fluid Mechanics Research*. 24(4-6): 707-715, 1997, doi: 10.1615/InterJFluidMechRes.v24.i4-6.260.
30. Senda, J., et al., "Measurement and Modeling on Wall Wetted Fuel Film Profile and Mixture Preparation in Intake Port of SI Engine," SAE Technical Paper 1999-01-0798, 1999, doi: 10.4271/1999-01-0798.
31. Chandra, S. and Avedisian, C., "The collision of a droplet with a solid surface," *Physics of Fluids A: Fluid Dynamics*. 2(9): 1525-1525, 1990, doi: 10.1063/1.4738846.

32. Pasandideh‐Fard, M., et al., "Capillary effects during droplet impact on a solid surface," *Physics of fluids*. 8(3): 650-659, 1996, doi: 10.1063/1.868850
33. Rioboo, R., Tropea, C., and Marengo, M., "Outcomes from a drop impact on solid surfaces," *Atomization sprays*. 11(2): 1-12, 2001, doi: 10.1615/AtomizSpr.v11.i2.40.
34. Yao, S.-C. and Cai, K.Y., "The dynamics and Leidenfrost temperature of drops impacting on a hot surface at small angles," *Experimental Thermal Fluid Science*. 1(4): 363-371, 1988, doi: 10.1016/0894-1777(88)90016-7.
35. Shirota, M., et al., "Dynamic Leidenfrost effect: relevant time and length scales," *Physical review letters*. 116(6): 064501, 2016, doi: 10.1103/PhysRevLett.116.064501.
36. Kandlikar, S.G. and Steinke, M., "Contact angles and interface behavior during rapid evaporation of liquid on a heated surface," *International Journal of Heat Mass Transfer*. 45(18): 3771-3780, 2002, doi: DOI: 10.1016/S0017-9310(02)00090-X.
37. Zhu, X., et al., *Investigation of the Effects of Heat Transfer and Thermophysical Properties on Dynamics of Droplet-Wall Interaction*. 2019, SAE Technical Paper.
38. *API Manual of Petroleum Measurement Standards. Chapter 11 - Physical Properties Data, Section 1: Temperature and Pressure Volume Correction Factors for Generalised Crude Oils*, in *Refined Products and Lubricating Oils*.
39. Chen, R. and Wang, H., "Effects of tangential speed on low-normal-speed liquid drop impact on a non-wettable solid surface," *Experiments in fluids*. 39(4): 754-760, 2005, doi: 10.1007/s00348-005-0008-6.

Contact Information

Seong-Young Lee

MEEM, Michigan Technological University
815 R.L. Smith Bldg.
1400 Townsend Drive
Houghton, MI 49931, USA
Phone: 906-487-2559
sylee@mtu.edu

Acknowledgments

This research was funded by the Department of Energy (DOE), Office of Energy Efficiency and Renewable Energy (EERE) and the Department of Defense, Tank and Automotive Research, Development, and Engineering Center (TARDEC), under Award Number DE‐EE0007292.

Nomenclature

$\boldsymbol{We}$	Weber number, $We = \rho u^2 d_o/\sigma_{lg}$
$\boldsymbol{Re}$	Reynolds number, $Re = u d_o/v$
$\boldsymbol{Oh}$	Ohnesorge number, $Oh = \sqrt{We}/Re$
$\boldsymbol{K}$	Mundo number, $K = WeOh^{-0.4}$
$\boldsymbol{Nu}$	Nusselt number, $Nu = c d_o/k$
$\boldsymbol{Pr}$	Prandtl number, $Pr = c_p \mu/k$
$\boldsymbol{E_{kine}}$	Kinetic energy, (J)
$\boldsymbol{E_{grav}}$	Initial gravitational potential energy, (J)
$\boldsymbol{E_{surf}}$	Initial surface energy of the droplet before impingement, (J)
$\boldsymbol{E_{adh}}$	Adhesion energy, (J)
$\boldsymbol{E_{vis}}$	Viscous dissipation, (J)
$\boldsymbol{E_{def}}$	Deformation energy, (J)
$\boldsymbol{E_{heat}}$	Heat energy, (J)
$\boldsymbol{E_{grav,i}}$	Gravitational potential energy after impingement, (J)
$\boldsymbol{g}$	Gravity acceleration, ($m \cdot s^{-2}$)
$\boldsymbol{V_o}$	Initial droplet volume, (m^3)
$\boldsymbol{V_b}$	Volume of the back side of the droplet, (m^3)
$\boldsymbol{V_f}$	Volume of the front side of the droplet, (m^3)
$\boldsymbol{u}$	Impact velocity in the gravity direction, ($m \cdot s^{-1}$)
$\boldsymbol{u_i}$	Mean velocity of the droplet during spreading stage, ($m \cdot s^{-1}$)
$\boldsymbol{u_i^o}$	Initial mean velocity, ($m \cdot s^{-1}$)

H_d Equivalent height of the dome, (m)

H_c Equivalent height of the cylindar, (m)

r_b Spreading length of back side of the droplet, (m)

s Displacement of geometric axis from the impinging point along the x direction, (m)

r Distance from geometric axis to the leading edge, (m)

s_m Maximum displacement of symmetry axis, (m)

r_m Maximum distance from geometric axis to the leading edge, (m)

$r_{b,m}$ Maximum spreading length of back side, (m)

h_m Height of the liquid film at the end of the spreading process, (m)

r_o Initial droplet radius, (m)

d_o Initial droplet diameter, (m)

$t_{b,m}$ The time maximum spreading length is acquired, s

h_{eff} Effective height, (m)

S_{def} Deformed surface area, (m^2)

S_{cap} Droplet surface of the spherical cap, (m^2)

S_b Droplet surface of the contact area between back side of the droplet and the wall, (m^2)

P Impinging point

q Heat transfer per unit time, ($J \cdot s^{-1}$)

c Heat transfer coefficient, ($W \cdot m^{-2} \cdot K^{-1}$)

c_p Specific heat at constant pressure, ($J \cdot kg^{-1} \cdot K^{-1}$)

k Thermal conductivity, ($W \cdot m^{-1} \cdot K^{-1}$)

t Real time, (s)

T_d Droplet temperature, (℃)

T_w Wall temperature, (℃)

T_s Saturation temperature, (K)

T_L Leidenfrost temperature, (K)

T_{BP} Boiling point temperature, (K)

Greek symbols

α Inclined angle of the wall, (°)

β_m Ratio of maximum spreading length to initial droplet diameter

θ_b Contact angle of trailing edge, (°)

θ_f Contact angle on leading edge, (°)

$\theta_{b,m}$ Contact angle of the trailing edge when maximum spreading length is acquired, (°)

σ_{lg} Surface energy density of diesel, ($J \cdot m^{-2}$)

ρ Density of diesel droplet, ($kg \cdot m^{-3}$)